FEASIBILITY FOR DETECTING LIVER METASTASES IN DOGS USING GADOBENATE DIMEGLUMINE-ENHANCED MAGNETIC RESONANCE IMAGING

ARNAUD LOUVET, ANNE-CAROLE DUCONSEILLE

Early detection of liver metastases may improve the prognosis for successful treatment in dogs with primary tumors. Hepatobiliary-specific contrast agents have been shown to allow an increase in magnetic resonance imaging (MRI) detection of liver metastases in humans. The purpose of this prospective study was to test the feasibility for using one of these agents, gadobenate dimeglumine, to detect liver metastases in dogs. Ten consecutive dogs known to have a primary tumor were recruited for inclusion in the study. All dogs were scanned using the same protocol that included a T2-weighted respiratory-triggered sequence, T1 VIBE, diffusion-weighted imaging, and 3D-FLASH before and after dynamic injection of gadobenate dimeglumine contrast medium. Delayed imaging was performed less than 30 min after injection and up to 60 min in two cases. Histological analysis of liver lesions identified in delayed phases was performed for each case and confirmed metastatic origin. In all cases, lesion number detected in hepatobiliary contrast-enhanced sequences was statistically higher than in other sequences. Optimal lesion detection occurred with a 3D-FLASH sequence acquired in the transverse plane and less than 30 min after injection. Findings indicated that gabobenate dimeglumine enhanced MRI is a feasible technique for detecting liver metastases in dogs. © 2014 *American College of Veterinary Radiology.*

Key words: dog, gadobenate dimeglumine, hepatobiliary-specific contrastmedium, liver, MRI.

Introduction

THE CANINE LIVER, as well as its human counterpart, is a principal site for primary malignancies and may be the most common site of metastasis from primary tumors elsewhere in the body.[1,2] Metastasis to the liver from nonhepatic neoplasia occurs 2.5 times more frequently than primary liver tumors in dogs, particularly from primary lesions of the spleen, pancreas, and gastrointestinal tract.[2] Currently, due to the grave prognosis, many canine owners opt to have their dogs euthanized if evidence of numerous metastatic lesions is found preoperatively. However, we hypothesize that palliative and possibly curative treatments for liver metastases in dogs, as in human medicine, will emerge in the near future.

Thanks to its high tissue contrast and the introduction of fast imaging techniques, magnetic resonance (MR) imaging has become an important tool in liver imaging in human medicine. Magnetic resonance imaging improves the detection and characterization of focal liver lesions when other modalities such as computed tomography (CT) and ultrasonography (US) do not provide conclusive findings.[3] In humans, up to 60% of liver metastases, especially those smaller than 10 mm, are missed at US or CT, and this substantially affects the effectiveness of surgical or nonsurgical treatments. The discovery of liver metastases is no longer an indication for terminal care. Improvements in chemotherapy continue, and surgical or nonsurgical ablative techniques of secondary lesions are a rapidly evolving. However, it is clear from surgical studies that the best outcome for liver surgery is achieved when the extent of the disease is still small and there is only a solitary lesion or the lesions are few in number.[4]

With the recent advent of hepatobiliary-specific contrast-agents, which are targeted to enhance hepatocytes, a further increase in accuracy of liver metastases detection has been reported in humans.[3] At the moment, two gadolinium-based contrast agents (GBCA) exhibit some hepatobiliary metabolism that differentiates them from standard extracellular agents. These GBCAs have the unique advantage for liver imaging of combining the properties of an extracellular agent (e.g. vascular phase imaging) with the advantages of a hepatobiliary-specific metabolism. The two currently approved agents are gadobenate dimeglumine, also kown as Gd-BOPTA (Multihance, Bracco SpA, Milan, Italy) and gadoxetate disodium, also known as Gd-EOB-DTPA

From the Centre d'Imagerie par Résonance Magnétique de l'Animal (CIREN), 80, rue Péreire, 78100, Saint-Germain-en-Laye, France.
Address correspondence and reprint requests to Arnaud Louvet, at the above address. E-mail: arnaudlouvet@noos.fr

Received April 18, 2014; accepted for publication November 4, 2014.
doi: 10.1111/vru.12237

(Eovist, EOB-Primovist, Bayer HeathCare, Wayne, NJ). Gd-EOB-DTPA has recently been found to be safe and efficient for liver enhancement in normal dogs using high-field magnets.[5] Nine cases were studied in another report using a low-field magnet for liver mass characterization but not for metastasis detection.[6] Currently, Gd-EOB-DTPA is commercially available only in a few European countries, and is more than twice the price of Gd-BOPTA. At the time of this writing, Gd-BOPTA was approved for central nervous system (CNS) applications in United States and for CNS and liver imaging in several countries outside the United States.[7] Gd-BOPTA contains a hydrophobic benzyloxymethyl group partly responsible for a weak and transient affinity for serum albumin.[8] This particularity has been assumed to be responsible for its greater signal enhancement than other GBCAs used at the same dosage. In addition, thanks to the chain containing the benzene ring selectively taken up by the so-called canalicular multispecific organic anion transporter, it confers to the molecule the ability to pass from blood through hepatocytes into the bile to an extent dependent on animal species. Plasma concentration-time profile, excretion pattern, distribution, and metabolism have been evaluated in animals, i.e. the rat, the rabbit, the dog, and the monkey.[9] Rats are the best biliary excretors followed by dogs, rabbits, and monkeys. Only monkeys show levels of biliary excretion (3–12% within 8 h after administration) as low as humans. In dogs, biliary excretion has been found to be around 32–43%. Biliary concentration of Gd-BOPTA peaks at 45–60 min after injection, however liver parenchyma enhancement begins earlier during the hepatocellular phase that precedes the biliary phase. A weak binding to intrahepatocytic macromolecular structures could be responsible as well for a greater signal enhancement.[3,10,11]

Objectives of the current study were threefold. The first aim was to test the hypothesis that Gd-BOPTA uptake will be higher and metabolized faster from dogs' hepatocytes than in humans and rapidly detected in the gallbladder and common biliary duct.

Second, to test the hypothesis that strongly hypointense, nodular, noncystic lesions identified in the postcontrast hepatocellular phase will most likely be metastases. Third, to test the hypothesis that the postcontrast hepatocellular phase will outperform conventional T1 and T2-weighted sequences as well as arterial, portal, and equilibrium phases of the dynamic injection for detecting metastatic liver lesions.

Materials and Methods

This study was designed as a single-center prospective study with histopathological control of the diagnostic accuracy of unenhanced and enhanced hepatobiliary phase for liver metastases detection and characterization. All procedures were approved by and conducted in accordance with requirements of an institutional animal care and use committee.

Animals

Between July 2012 and December 2013, 10 consecutive privately owned dogs (six males and four females, aged seven to 13 years with a mean age of 12 years) were recruited. All dogs had surgically proven or biopsy proven primary and metastatic liver lesions that were initially suspected at conventional US. In all cases, US examination identified a primary mass lesion and no or nonspecific focal liver abnormalities.

MR Imaging

With informed owner consent, all included dogs underwent Gd-BOPTA-enhanced MR imaging. Magnetic resonance examinations were performed with a 1.0 Tesla magnet (MAGNETOM HARMONY, upgrade MAESTRO, Siemens Medical solutions, Malvern, PA) with high performance gradients (33 mT/m). The MRI liver examination procedure was adapted from a previously published basic protocol in human medicine and included T2-weighted respiratory triggered sequences, T1-weighted before and after contrast-medium injection, diffusion-weighted imaging, dynamic-enhanced T1-weighted sequences, and T1-weighted delayed sequences.[12] Dogs were premedicated with an intramuscular injection of 0.04 ml/kg buprenorphine (Buprecare 0.3 mg/ml, Axience, Pantin, France) and 0.01 ml/kg acepromazine (Calmivet 5 mg/ml, Vetoquinol, Lure, France) 30 min before the induction. Anesthesia was induced with 0.2 ml/kg intravenous propofol (Propovet 10 mg/ml, Axience, Pantin, France) and then maintained with isoflurane (IsoFlo 1 ml/ml, Axience, Pantin, France) and oxygen. The dogs were in dorsal recumbency. For dogs weighting less than 10 kg, an emitting-receiving extremity circular polarization coil was used. When the weight of the dog did not allowed the use of the extremity coil, the cranial abdomen was imaged with the association of a dorsal phased-array spine coil and a ventrally placed body coil working in parallel. Breath-holding was induced by intravenous injection of 0.04 ml/kg atracurium besilate (Tracrium 25 mg/2.5 ml, GlaxoSmithKline, Marly le Roi, France) at the beginning of the examination. Breathing was manually assisted between each sequence acquisition. Apnea was reversed at the end of the procedure using 0.04 ml/kg atropine (Atropine 1 mg/ml, Lavoisier, Paris, France) followed by 0.04 ml/kg neostigmine (Prostigmine 0.5 mg/ml, MEDA Pharma, Paris, France).

Precontrast sequences were a T1-weighted three-dimensional Fast-Low-Angle-Shot in the transverse plane (3D-FLASH: TR 6.29 ms, TE 2.12 ms, flip angle 30°, Nex 2,

slice thickness 3.6 mm, FOV 176 × 220 mm, Matrix: 189 × 320, bandwidth 460 Hz/pixel, 48 slices per slab, acquisition time 45 s) and Volume-Interpolated-Breath-hold Examination (VIBE: TR 9.41 ms, TE 3.5 ms, Nex 2, flip angle 25°, slice thickness 3.6 mm, FOV 187 × 250 mm, Matrix 175 × 256, bandwidth 280 Hz/pixel, 40 slices per slab, acquisition time 52.7 s) in the transverse and dorsal plane.

A proprietary fluoroscopic contrast-medium detection sequence (CARE BOLUS ®) was used in the dorsal plane centered in the cranial part of the abdominal aorta. Gd-BOPTA (Multihance 0.5 mmol/ml, Bracco, Evry, France) was injected manually through a 22-G catheter placed into the cephalic vein and equipped with a 20 ml extension set at 0.4 ml/kg (0.2 mmol/kg) at an approximate rate of 2 ml/s and followed by a 20 ml of 0.9% saline flush.

Dynamic injection was started as soon as contrast media appeared in the cranial abdominal aorta. In all patients (10/10), four sequences were acquired in the arterial phase, the portal phase (45 s postinjection), equilibrium (100 s postinjection), and hepatobiliary phase (20 min postinjection). The time interval between the equilibrium phase and the hepatobiliary phase was used to perform a T2-weighted turbo-spin–echo (TSE) respiratory trigged sequence in the transverse plane (TR 5130 ms, TE 66 ms, slice thickness 3.6 mm, Echo Train Length 11, flip angle 150°, Nex 3, FOV 232 × 290 mm, Matrix 308 × 384, acquisition time 7 min 26 s), diffusion-weighted images in the axial plane (b0, b50, b300), and T1-VIBE sequences in the axial and dorsal plane. In only two cases (2/10), a very-delayed transverse 3D-FLASH sequence was acquired 60 min after contrast-medium injection. Breathing was manually assisted by the author (A.L.) during the T2-weighted respiratory trigged sequence to keep thoracic motion as regular as possible in order to obtain images of consistent high quality and to keep the examination time as short as possible.

Image Evaluation

Image analysis was performed by the first author (A.L., 6 years experience in abdominal MRI). The observer was unaware of the histopathological nature of the primary neoplasia, but was informed of the previous ultrasound examination and thus the lesion location. Arterial, portal, equilibrium, and hepatobiliary phases were subtracted using the embedded workstation software (NUMARIS/4 Syngo MR A35, Siemens AG, 2009) from the initial preinjection 3D-FLASH sequence in order to decrease the spontaneously high signal from fat without increasing acquisition time associated with implementation of a fat-saturation module.

Hepatobiliary sequences were examined first; hypointense lesions were identified, localized, and considered subjectively as strongly, moderately, or slightly hypointense to the adjacent liver parenchyma. Every lesion was then localized in the earliest 3D-FLASH sequences (arterial, portal, and parenchymal-equilibrium) T1-VIBE and T2-weighted TSE transverse sequence. Nodular lesions that appeared strongly hyperintense in T2-weighted, hypointense in T1-weighted FLASH or VIBE and without any contrast enhancement were strongly suspected to be of cystic nature and were excluded from further analyses, even when they appeared in strong hypointense signal in hepatobiliary phase. Every lesions that appeared moderately and strongly hypointense, or more hypointense in the hepatobiliary phase were recorded as possible metastases. Lesion number detected on each set of sequences was recorded. When this number exceeded 60, it was assigned an arbitrary value of 60 because the exact count was judged approximate.

Statistical Analysis

Statistical tests were performed by one author (A.L.) and a university statistician. The first author (A.L) drew one circular region of interest (ROI) using a commercial PACS system (OsiriX v.4.1.2 32-bit) in the normal-appearing liver parenchyma on the hepatobiliaryT1-weighted 3D-FLASH image. The location of the ROI was then automatically registered on each set of images acquired before and after contrast medium injection and a ROI of similar size was drawn on each image. Resultant data were used to create a time-intensity curve illustrating the degree of enhancement of the liver parenchyma. For each time point, average signal-intensity was calculated, signal intensity ratio (postcontrast/precontrast), as well as standard deviation using Excel software. One-way ANOVA was then calculated between each time-point using commercially available software (Microsoft® Excel® for Mac 2011, v.14.3.9). The assumption of normality tested using the Shapiro–Wilk statistic, was met.

In order to compare the number of lesions detected in each different sequence, a Friedman rank sum test was conducted, the null hypothesis being that the lesion number detected for each sequence was the same. Pairwise testing was then conducted to compare T1-hepatobiliary with other sequences. All test results were evaluated using a significance level of $P < 0.05$.

Reference Standard

For all comparisons, histological, or cytological confirmation of at least one suspected liver metastasis was used as the reference standard. Confirmation was based on an ultrasound-guided biopsy (four cases), surgery (five cases), or postmortem examination (one case) performed the same day or less than 10 days after the MRI examination. Cytological (four cases) and histological confirmation (six cases) of the primary lesion was also obtained during

the same procedure. The sites for collecting lesion samples were chosen based on recorded MRI characteristics of metastasis and location accessibility. Not all MRI lesions were histopathologically or cytologically sampled. For purposes of this study, it was assumed that every lesion with similar MRI characteristics in all imaging sequences in a given dog was the same as the sampled lesion. A board-certified veterinary pathologist interpreted all histological and cytological samples.

Results

All focal liver lesions that were detected using MRI and sampled confirmed neoplastic infiltration, with no false-positive diagnoses. Among the 10 included dogs, two dogs had confirmed liver metastases from adrenal adenocarcinoma, one from hepatocellular carcinoma, one from hepatic carcinoid, one from renal fibrosarcoma, one from mediastinal undifferentiated soft tissue sarcoma, one from hepatic hemangiosarcoma, one from splenic hemangiosarcoma, one from pancreatic insulinoma, and one from gastric adenocarcinoma. Primary tumors confirmed histologically were hepatic carcinoid, renal fibrosarcoma, pancreatic insulinoma, hepatic hemangiosarcoma, splenic hemangiosarcoma, hepatocellular carcinoma. Primary tumors confirmed cytologically were adrenal adenocarcinoma, gastric adenocarcinoma, mediastinal soft-tissue undifferentiated sarcoma. In the hepatocellular carcinoma case, the largest lesion identified using MRI was presumed to be the primary tumor. In the hepatic carcinoid case, all masses were approximately the same size and the neoplastic involvement was deemed multifocal. In the hepatic hemangiosarcoma case, the primary liver tumor was presumed to be the largest lesion in the absence of the involvement of other abdominal organs.

The quality of all images acquired before and after Gd-BOPTA injection was considered to be excellent. No adverse effects from contrast medium administration were observed. In the normal appearing portions of the liver, signal intensity ratios strongly increased 45 s after contrast medium injection, then proceeded with a slightly ascending slope to reach a level roughly four to five times higher than the precontrast signal at 23 min followed by a slight decrease at 60 min (Fig. 1). Contrast enhancement could be detected in all (10/10) patients in the gallbladder and appeared on an average of 14.8 min (SD 4.3, 8–19 min) after intravenous contrast injection. In all cases, the T1-FLASH acquired at 23–24 min after injection depicted a large number of focal lesions that were not visible in T1-FLASH and T1-VIBE before contrast injection or during arterial phase of the dynamic injection. Among all of the cases in which metastases were found in hepatobiliary sequences, 7/10 cases were negative in T1-FLASH before contrast, 5/10 cases were negative in T1 VIBE after contrast medium injection, 4/10 cases were negative in T2 TSE, and 4/10 cases were negative in the arterial phase of the dynamic injection. Portal and equilibrium phases were (10/10) positive for the detection of focal lesions in all cases (10/10). A higher number of lesions was detected in hepatobiliary sequences compared to portal phase (37.2 vs. 13.1, $P < 0.005$) and equilibrium phase (37.2 vs. 30.8, $P = 0.025$) sequences (Appendix 1, Fig. 2). Subjective contrast between normal appearing liver parenchyma and liver focal lesions was consistently highest during the hepatobiliary phase (Fig. 3). Lesion conspicuity was subjectively better during the hepatobiliary phases than during the arterial, portal or equilibrium phases (Fig. 4). Liver enhancement was sufficiently marked in hepatobiliary phases that, in eight of our 10 patients, detection of lesions less than 2 mm in diameter with strong hypointense signal was possible. These small lesions were so numerous that an exact count was not possible (Fig. 5).

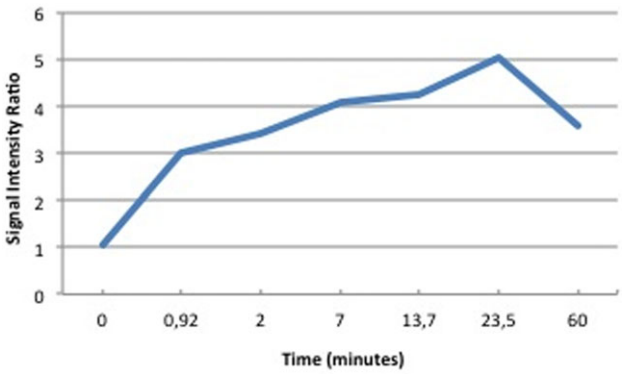

FIG. 1. Graphic representation of mean signal intensity ratios for background liver measured using regions of interest placed in transverse 3D-FLASH images acquired after intravenous administration of 0.2 mmol/kg gadobenate dimeglumine in 10 dogs. Measures were obtained at the arterial phase (0), portal phase (0.92 min), equilibrium phase (2, 7, and 13.7 min) and hepatobiliary phase (23.5 min) in 10 patients and very-delayed phase (60 min) in only two cases. Note that signal intensity ratio slightly increased between 7 and 23.5 min then decreased at 60 min.

Discussion

Findings from the current study indicated that (1) 0.2 mmol/kg Gd-BOPTA is a safe and feasible contrast-agent for strongly increasing the signal of the liver parenchyma in a time-delay compatible with clinical application in anesthetized dogs, (2) imaging dogs at 23–25 min postinjection provides similar information to imaging at 60 min postinjection, (3) a time-delay of 23–25 min postinjection probably matches the hepatocellular phase of the contrast-agent, and (4) the hepatobiliary phase sequence following Gd-BOPTA administration is optimal for depicting the greatest number of focal lesions with the highest contrast compared to earliest dynamic and conventional T1 and T2-weighted sequences.

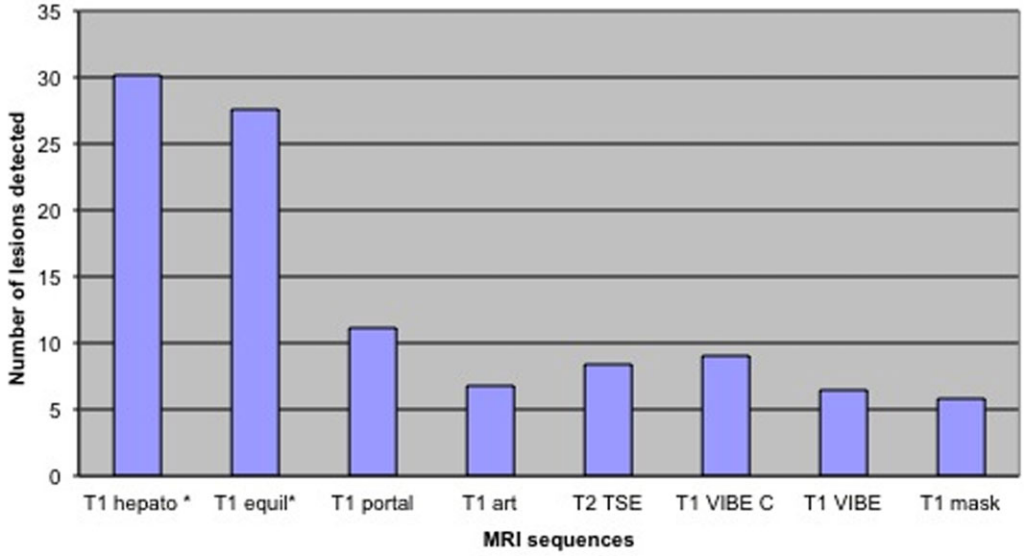

FIG. 2. Graphic representation of the mean number of lesions detected on different magnetic resonance imaging sequences for 10 dogs. ∗Denotes a significant difference compared to T1 hepatobiliary phase. T1 hepato, 3D-FLASH hepatobiliairy phase, T1 equil, 3D-FLASH equilibrium phase, T1 portal, 3D-FLASH portal phase, T1 art, 3D-FLASH arterial phase, T2 TSE, T2-weighted turbospinecho sequence, T1 VIBE C, T1-VIBE postinjection of Gd-BOPTA, T1 VIBE, T1-VIBE preinjection of contrast-medium, T1 mask, 3D-FLASH before injection of contrast-medium.

Findings differed from previous human studies in that delayed imaging for the hepatobiliary or hepatocellular phase of Gd-BOPTA has been reported to be 60–90 min after contrast injection.[13] Pharmacokinetic studies have found evidence that biliary elimination is larger and quicker in dogs.[8] In dogs, biliary excretion has been found to be around 29% and absolute bile MR signal intensity was found to occur around 15 min after injection in T1-weighted spin-echo sequences. Our personal observations in the current study were in accordance with these findings in that SI ratios were four to five times higher at 23 min after injection than those at the baseline. No significant difference in SI ratio values was found between 23 and 60 min for the dogs in the current study. Moreover, in all dogs, contrast medium could be seen in the gallbladder or the common biliary duct as soon as 14–16 minutes after injection, thus supporting our hypothesis that the liver uptake and elimination that must precede its excretion in the biliary ducts is quicker than in humans. In humans, Gd-BOPTA has been found to appear in the bile 20 min after the injection.[14]

The upper end dose of the contrast-medium used in this study has been recommended for cardiac imaging in animals[9] and no side-effect or anaphylactoid reaction such as recently described with lower doses were observed in our patients.[15] The main role of hepatobiliary-specific contrast agents is to improve both detection and characterization of lesions. Extracellular contrast-agents are less suitable for lesion detection because they affect both the normal liver parenchyma and the lesion equally. We hypothesized that, by increasing the contrast between the markedly enhanced normal parenchyma and the hypo or unenhanced lesions, hepatobiliary-specific contrast-agents may improve the detection of smaller masses in dogs. Several human studies have shown that contrast-enhanced MR imaging with a hepatobiliary-specific agent depicts more colorectal metastatic lesions in the liver than contrast-enhanced MRI with an extracellular fluid agent does and also adds diagnostic information and confidence. In the published literature, many studies of lesion detection with hepatobiliary-specific contrast agents focus on colorectal metastases. Data with regard to the detection of other metastases are currently limited but the rationale for significant differences is poor given that by definition all metastatic lesions are devoid of functional hepatic cells. Our results supported this hypothesis given the lack of signal difference regarding the tissue of origin of the metastases.

It should be understood that a hypointense signal in a lesion during the equilibrium phase of the dynamic injection and during the hepatocellular phase indicates different information. A lesion appearing with hypointense signal during the equilibrium phase means that the nonspecific tissue uptake by the lesion is inferior to the normal liver background and is an indirect reflexion of the pattern of its vascularisation. A lesion appearing with hypointense signal during the hepatobiliary phase of the contrast-medium means that it contains no, or very few, functional hepatocytes. Thus even if all metastatic lesions should theoretically appear with hypointense signal in hepatobiliary phase, the same is not always true during the equilibrium phase. Some hepatic metastases can exhibit hypointense signal, hyperintense signal, or near isointense signal in dynamic phases.[16] Conversely, some benign lesions could exhibit isointense

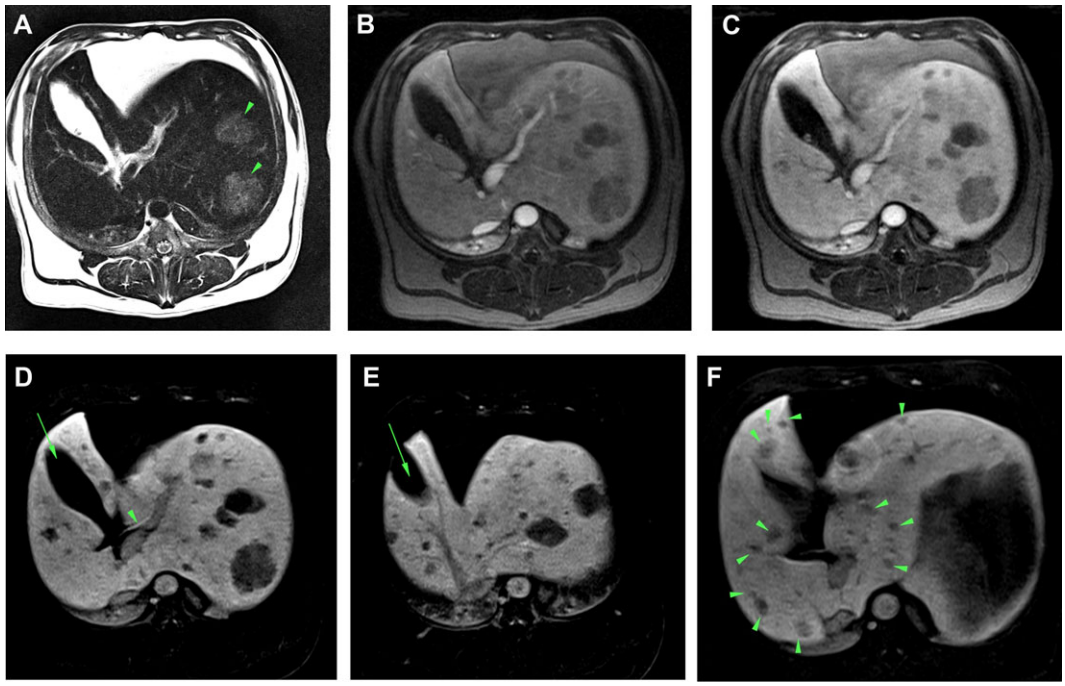

FIG. 3. Magnetic resonance imaging of the liver from a 14-year-old male Griffon crossed dog with hepatic carcinoid. A previous US examination (not shown) depicted only 2 focal lesions and a surgical treatment was an option; MRI with Gd-BOPTA was performed to confirm the paucity of lesions and the nonhepatocellular composition of the suspected lesion.

(A) Transverse T2-weighted TSE (TR = 5130 ms, TE = 66 ms, flip angle 150°) image demonstrating two hyperintense focal lesions (arrowheads). (B) Transverse 3D-FLASH (TR = 6.29 ms, TE = 2.12 ms, flip angle 30°) portal phase MR image shows several other lesions hypointense to the enhancing liver. (C) Transverse 3D-FLASH acquired during the equilibrium phase (+2 min).

(D–F) Transverse 3D-FLASH hepatocellular phase (+20 min) showing numerous hypointense well-defined lesions. The total count of hypointensities in hepatobiliary images exceeded 60, only five lesions were identified in the T2-weighted and T1-VIBE postcontrast images. Note in (D) and (E) the gallbladder (arrow) and common biliary duct with hyperintense contrast-medium (arrowhead). Note in (F) the high number of focal hypointense lesions throughout the hepatic parenchyma (arrowheads).

signal during the equilibrium phase and isointense signal in the hepatobiliary phase if they contain sufficient functional hepatocytes (classic form of focal nodular hyperplasia in humans). In 6/10 cases of the current study, the number of hepatic lesions detected in hepatobiliary phases was higher than in equilibrium phases meaning that some lesions in this phase of the dynamic injection had isointense signal to the adjacent parenchyma, thus would be potentially missed if the hepatobiliary sequence was not performed. Authors therefore believe that examination, and thus acquisition of all sequences of the protocol is indispensable because accurate characterization of a focal lesion will rely on its behaviour during the arterial, portal, and equilibrium phases of the dynamic injection as well as its signal intensity in noncontrast and T2-weighted sequences. For example, a cystic lesion will be similar in appearance to a metastasis in hepatobiliary sequence, but commonly in a strongest hypointense signal in T1-weighted before contrast, strongest hypersignal in T2-weighted signal with no enhancement in arterial, portal, or equilibrium phases.

The 3D-FLASH sequence used here has been mainly used for contrast-enhanced angiography in several recent veterinary studies.[17,18] Our personal experience was that signal intensity of the liver in delayed-hepatobiliary phases was strongly superior to the frequently used T1-weighted VIBE sequence for this purpose in human liver imaging. The VIBE sequence is a 3D radio-frequency-spoiled gradient echo sequence modified to obtain a small slice thickness (around 2–3 mm) covering large anatomic areas (typically 80 partitions or slices) in a fast imaging time (typically less than 30 s). The main characteristic of this sequence is an asymmetric sampling in the section-select direction (kz) allowing a reduction in the number of phase-encoding steps in this direction.[19] Slice thickness, pixel size, repetition time, echo time, and flip angle were not very different between 3D-FLASH and 3D-VIBE sequences (3.6 and 2.8 mm, 1.0 × 1.45 and 0.94 × 1.2 mm, 6 and 9 ms, 2.1 and 3 ms, 30° and 25°, respectively). The gain in imaging time (28 ms vs. 43 ms for VIBE and FLASH, respectively) was not a primary objective for nonbreathing curarized animals and the acquisition time of 43 ms of the 3D-FLASH enabled sufficient temporal-resolution to acquire data during selected periods of enhancement (e.g. hepatic arterial phase vs. portal venous phase). Although not investigated here, the reason why 3D-FLASH sequence performed better than the 3D-VIBE sequence could be the topic of another study.

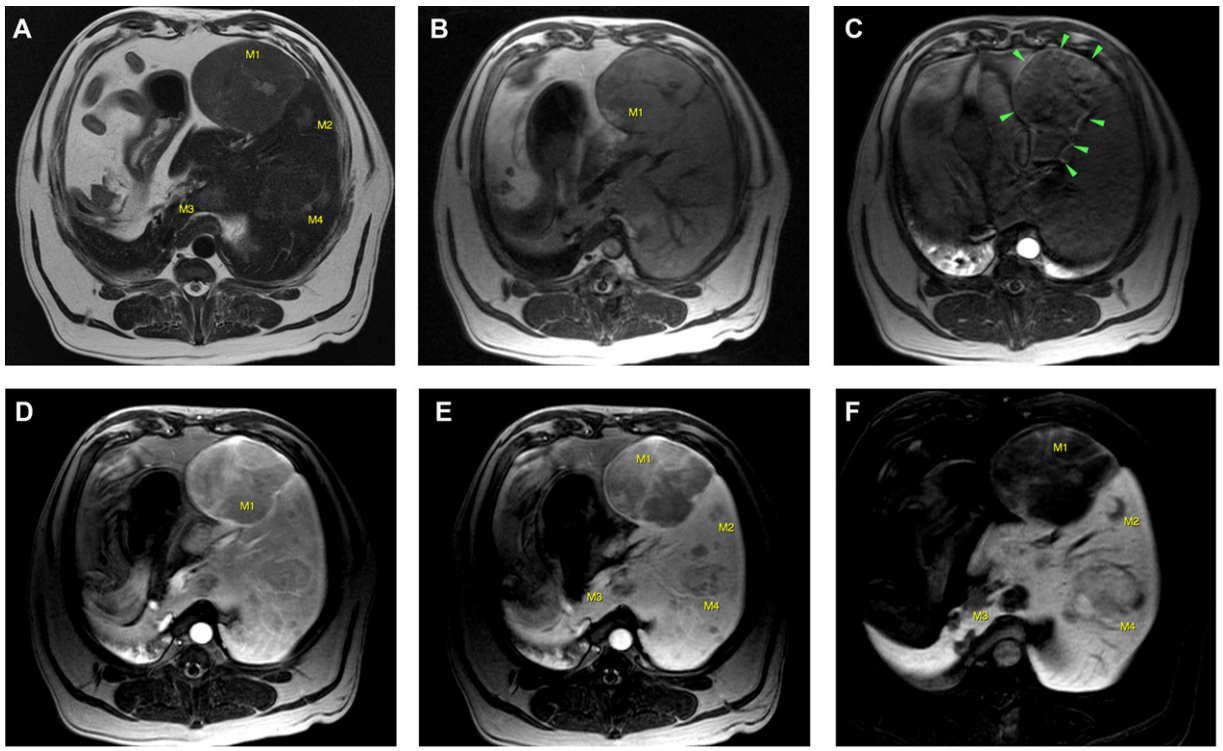

FIG. 4. Magnetic resonance imaging of the liver from a 12-year-old Golden Retriever dog with hepatocellular carcinoma. Previous US examination found two focal lesions corresponding to M1 and M4 in these images with the same hyperechoic slightly heterogeneous appearance and Gd-BOPTA MRI was performed to characterize these two lesions and possibly detect other lesions.

(A) Transverse T2-weighted TSE (TR = 5130 ms, TE = 66 ms, flip angle 150°) image confirmed the presence of the main two lesions (M1 and M4) detected with US and identified at least four other focal ill-defined areas of hyperintensity. (B) Transverse 3D-FLASH (TR = 6.29 ms, TE = 2.12 ms, flip angle 30°) before contrast-medium injection. (C) Transverse 3D-FLASH arterial phase showed a patchy intratumoral and continuous peripheral enhancement of M1 with a serpentine small arterial vessel feeding the mass (arrows). M4 was not enhancing. (D–E) Transverse 3D-FLASH portal and equilibrium phases showed heterogeneous enhancement of M1 and M4. Numerous other hypointense lesions were identified. (F) Transverse 3D-FLASH subtracted in hepatocellular phase (+20 min) showed numerous hypointense lesions (M2, M3) allowing accurate detection of other lesions. M1 was strongly hypointense to the background liver allowing confirmation of this lesion as a nonfunctioning hepatocellular tumor. Hepatocellular carcinoma emanating from M1 was histologically proven as well from a smaller satellite lesion suspect to be M2 from the same lobe. M4 retained contrast medium and was suggestive of a benign mass composed of functioning hepatocytes (not histologically proven).

We observed as well that diffusion-weighted sequences did not allow detection of most of the metastases identified in hepatocellular phase. The reasons for this discrepancy are not currently known but relate probably to our imaging sequence design and magnet properties.[20] In humans, liver diffusion-weighted imaging has been reported to have multiple possible applications, particularly for lesion detection and characterization with better results compared to those of T2-weighted sequences[21] but sometimes conflicting value to contrast-enhanced delayed imaging.[22] Further studies will thus be necessary to confirm these results in small animals.

There are some limitations to the study. The first was the small size of our study group and particularly the fact that the signal intensity ratio at 60 min was only available in two cases. The fact that our patients were anesthetized did not enable us to lengthen the examination time in order to statistically demonstrate our observations and future studies dedicated to this subject will be necessary. Secondly, every lesion considered to be metastatic in MRI was not histologically proven because of the practical inability to sample the frequently large number of lesions detected in alive and even deceased patients. Moreover, in the majority of patients and because of the multiplicity and the small size of the lesions, we could not be sure that sampled lesions corresponded to the same lesions identified in the MRI examination. Care was taken to confirm that sampled and nonsampled lesions were behaving similarly in all imaging sequences of the protocol. However, authors acknowledge that all strongly hypointense focal lesions identified in hepatobiliary phase cannot be doubtlessly determined as metastases, but only as lesions that do not contain functioning hepatocytes. A known primary tumor should increase the probability of a metastatic lesion. All of the consecutive patients included in this study had to have a primary tumor associated with focal, nonspecific abnormalities in liver ultrasound. All cases showed focal lesions in the hepatobiliary sequences, and were confirmed to have at least one

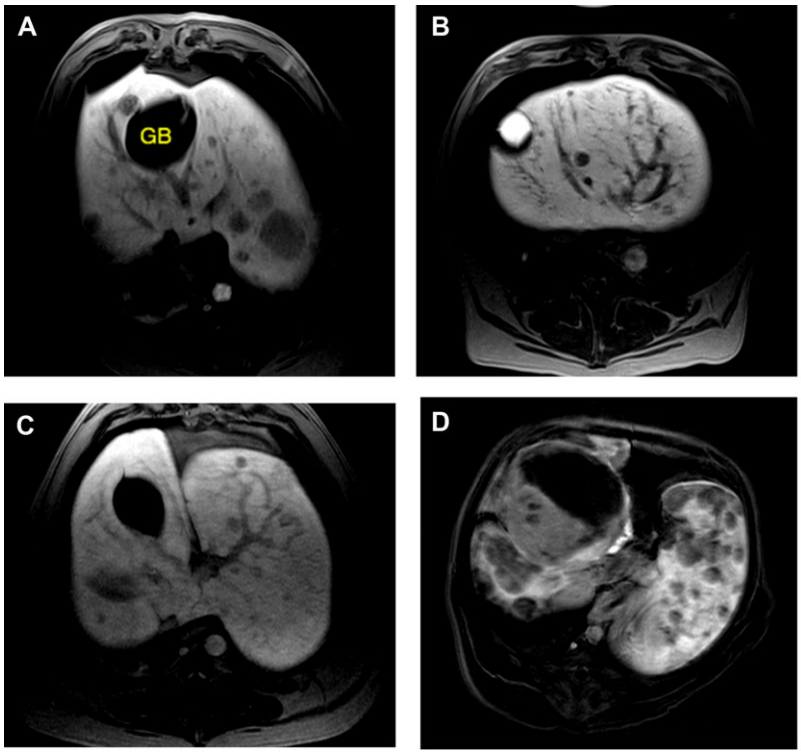

FIG. 5. Transverse 3D-FLASH (TR = 6.29 ms, TE = 2.12 ms, flip angle 30°) hepatobiliary phase (+23 min) Gd-BOPTA-enhanced MR imaging of the liver of primary-tumor bearing dogs. (A) Seven-year-old Siberian husky dog with a mediastinal undifferenciated soft-tissue sarcoma. (B) Twelve-year-old Crossed breed dog with right adrenal adenocarcinoma. (C) Nine-year-old Labrador Retriever dog with renal fibrosarcoma. (D) Thirteen-year-old American cocker spaniel dog with hepatic hemangiosarcoma. Each of these images shows high contrast and good delineation of lesions against strongly enhancing liver parenchyma. Liver metastases were histologically proven in each of these patients. GB. Gallbladder. Note in (B) the gallbladder filled with contrast medium.

lesion to be metastatic in nature. This seemingly very high incidence should be considered further, keeping in mind selection bias (the owner's agreement to allow the performance of an MRI examination, presence of nonspecific liver abnormalities in ultrasound) and confirmed by future studies.

The third limitation of the current study was the assumption that enhancing liver, in contrast to the focal lesion, was actually an ROI composed of normal functioning hepatocytes. Some studies have shown that quantifying liver enhancement could be a means of assessing liver functional reserve implicating a correlation between signal intensity and liver function. In this case, we could argue that differences in time-intensity curves would be partly explained by differences in liver function between animals. However, signal intensity ratio at each time-point during the dynamic injection did not show considerable spreading of the data despite the great difference in the patients' medical conditions, age, weights. It seems intuitive and probable that the contrast between a focal lesion devoid of functional hepatocytes and the adjacent parenchyma will be stronger in a normal functioning liver and weaker in a failing liver.

Comparisons with extracellular fluid contrast agents was not performed in the current study because these data have been extensively studied in human diagnostic imaging. Currently available extracellular contrast-agents are not known to have hepatobiliary metabolism conferring them an interest for delayed imaging. Comparison with other less invasive and expensive imaging was also not performed in the current study. This has been done in several studies of humans, with some recent consideration of Gd-BOPTA enhanced MRI being the gold standard for hepatic metastases from colorectal cancer detection.[23–25] We acknowledge that contrast-enhanced US has been used in humans and dogs for this purpose.[26] Contrast-enhanced US suffers from limitations, one being difficulty imaging the whole liver due to anatomical inaccessibility, and another being equipment and operator dependency.

Currently, liver mass characterization is the most established and successful indication of contrast-enhanced US but not considered the best imaging technique for early detection of liver metastases in humans.[20–24]

In conclusion, findings from this study indicated that gadobenate dimeglumine-enhanced MR imaging is a safe and feasible technique for detection and characterization of liver metastases in dogs known to have a primary tumor and with suspected or equivocal liver metastases on ultrasound. Future studies are needed to

determine whether this technique improves management of surgical or nonsurgical patients as well as providing new data for defining prognosis. Authors recommend using an upper end dose of the contrast medium, 23–25 min delayed imaging with 3D-FLASH sequences in the transverse plane. Arterial, portal and parenchymal-equilibrium imaging, as well a T2-weighted TSE can be performed with the same contrast-agent. Because Gd-BOPTA hepatobiliary uptake and elimination are unique in dogs, an imaging delay of 60 min may not be necessary as in humans. Further studies are needed to confirm these preliminary findings.

APPENDIX 1. Pathological Diagnoses and Number of Liver Focal Lesions Detected Using Different MRI Sequences for Each of 10 Dogs with Confirmed Primary Tumors

Case no.	Pathological diagnosis	T1 mask*	T1 VIBE	T1 VIBE+C	T2 TSE	T1 art	T1 portal	T1 equil	T1 hepato
1	Hepatic carcinoid	0	3	5	5	2	11	>60	>60
2	Adrenal adenocarcinoma	1	2	13	7	2	10	15	15
3	Thoracic undifferentiated soft tissue sarcoma	0	2	6	8	3	6	>60	>60
4	Adrenal adenocarcinoma	0	1	2	5	0	10	40	>60
5	Hepatic hemangiosarcoma	>60	>60	>60	>60	>60	>60	>60	>60
6	Gastric adenocarcinoma	0	0	0	0	0	2	5	11
7	Hepatocellular carcinoma	1	0	1	0	3	4	10	10
8	Renal fibrosarcoma	0	0	3	0	0	5	23	30
9	Pancreatic insulinoma	0	0	1	0	1	3	5	6
10	Splenic hemangiosarcoma	0	0	2	3	0	20	30	>60
	mean	6.2	6.8	9.3	8.8	7.1	13.1	30.8	37.2
	Friedman rank sum test comparison†	$P = 0.0027$*	$P = 0.0027$*	$P = 0.0027$*	$P = 0.0027$*	$P = 0.0027$*	$P = 0.0027$*	$P = 0.025$*	

*T1 mask, 3D-FLASH before injection of contrast-medium; T1 VIBE, T1-VIBE before injection of contrast-medium; T1 VIBE+C, T1-VIBE postinjection of Gd-BOPTA; T2 TSE, T2-weighted turbospinecho sequence; T1 art, 3D-FLASH arterial phase; T1 portal, 3D-FLASH portal phase; T1 equil, 3D-FLASH equilibrium phases; T1 hepato, 3D-FLASH hepatobiliary phase.
†Asterisk denotes a significant difference compared to T1 hepatocellular phase.

REFERENCES

1. Ananthakrishnan A, Gogineni V, Saeian K. Epidemiology of primary and secondary liver cancers. Semin Intervent Radiol 2006;23: 47–63.

2. Cullen JM, Propp JA. Tumors of the liver and gall bladder. In: Meuten DJ (ed): Tumors in domestic animals, 4 ed, Ames, Iowa: Iowa state press, 2002.

3. Del Frate C, Bazzochi M, Mortele K.J., et al. Detection of liver metastases: comparison of gadobenate dimeglumine and ferumoxides-enhanced MR Imaging examinations. Radiology 2002;225:766–772.

4. Robinson PJ. The early detection of liver metastases. Cancer Imaging 2002;2:1–3.

5. Marks AL, Hecht S, Stokes JE, Conklin GA, Deanna KH. Effects of gadoxetate disodium (EOVIST®) contrast on magnetic resonance imaging characteristics of the liver in clinically healthy dogs. Vet Radiol Ultrasound 2014,55:286–291.

6. Yonetomi D, Kadosawa T, Miyoshi K, et al. Contrast agent Gd-EOB-DTPA (EOB Primovist ®) for low-field magnetic resonance imaging of canine focal liver lesions. Vet Radiol Ultrasound 2012;53:371–380.

7. Leyendecker JR, Brown J, Merkle EM. Section I.4: using magnetic resonance contrast agents in the abdomen and pelvis. In: Leyendecker JR, Brown J, Merkle EM (eds): Practical guide to abdominal and pelvic MRI, 2nd ed. Philadelphia, USA: Wolters Kluwer, 2011;41–62.

8. de Haën C, La Ferla R, Maggioni R. Gadobenate dimeglumine 0.5M solution for injection (Multihance © as contrast agent for magnetic resonance imaging of the liver: mechanistic studies in animals. J Comput Assist Tomogr 1999;23(Suppl. I): S169–S179.

9. Lorusso V, Arbughi T, Tirone P, de Haën C. Pharmacokinetics and tissue distribution in animals of gadobenate ion, the magnetic resonance imaging contrast enhancing component of gadobenate dimeglumine 0.5M solution for injection (Multihance ®). J Comput Assist Tomogr 1999;23(Suppl. 1):S181–S194.

10. Liang J, Sammet S, Yang X, Jia G, Takayama Y, Knopp MV. Intraindividual in vivo comparison of gadolinium contrast agents for pharmacokinetic analysis using dynamic contrast enhanced magnetic resonance imaging. Invest Radiol 2010;45:233–244.

11. Cavagna FM, Dapra M, Castelli PM, Maggioni F, Kirchin MA. Trends and developments in MRI contrast agent research. Eur Radiol 1997;7(Suppl.5):S222–S224.

12. Leyendecker JR, Brown J, Merkle EM. Section I.6: abdominal and pelvic protocol basics. In: Leyendecker JR, Brown J, Merkle EM (eds): Practical guide to abdominal and pelvic MRI, 2nd ed. Philadelphia, USA: Wolters Kluwer, 2011;82–103.

13. Petersein J, Spinazzi A, Giovagnoni A, et al. Focal liver lesions: evaluation of the efficacy of gadobenate dimeglumine in MR

imaging–a multicenter phase III clinical study. Radiology 2000;215: 727–736.

14. Seale MK, Catalano OA, Saini S, Hahn PF, Sahani DV. Hepatobiliary-specific MR contrast agents: role in imaging the liver and biliary tree. Radiographics 2009;29:1725–1478.

15. Girard NM, Leece EA. Suspected anaphylactoid reaction following intravenous administration of gadolinium-based contrast agent in three dogs undergoing magnetic resonance imaging. Vet Anaesth Analg 2010,37: 352–356.

16. Pedro MS, Semelka RC, Braga L. MR imaging of hepatic metastases. MRI Clin North Am 2002;10:15–29.

17. Mai W. Multiphase time-resolved contrast-enhanced portal MRA in normal dogs. Vet Radiol Ultrasound 2009;50:52–57.

18. Bruehschwein A, Foltin I, Flatz K, Zoellner M, Matis U. Contrast-enhanced magnetic resonance angiography for diagnosis of portosystemic shunts in 10 dogs. Vet Radiol Ultrasound 2010;51: 116–121.

19. Lee VS, Lavelle MT, Rofsky NM, et al. Hepatic MR imaging with a dynamic contrast-enhanced isotropic volumetric interpolated breath-hold examination: feasibility, reproducibility and technical quality. Radiology 2000;215:365–372.

20. Heijmen L, ter Voert EEGW, Nagtegaal ID, et al. Diffusion-weighted MR imaging in liver metastases of colorectal cancer: reproducibility and biologic validation. Eur Radiol 2013;23:748–756.

21. Taouli B, Koh DM. Diffusion-weighted MR imaging of the liver. Radiology 2010;254:47–66.

22. Fu GL, Du Y, Zee CS, et al. Gadobenate dimeglumine-enhanced liver magnetic resonance imaging: value of hepatobiliary phase for the detection of focal liver lesions. J Comput Assist Tomogr 2012;36:149.

23. Cantisani V, Ricci P, Erturk M, et al. Detection of hepatic metastases from colorectal cancer: prospective evaluation of gray scale US versus SonoVue ® low mechanical index real-time enhanced US as compared with multidetector-CT or Gd-BOPTA-MRI. Utraschall Med 2010;31:500–505.

24. Blyth S, Blakeborough A, Peterson M, Cameron IC, Majeed AW. Sensitivity of magnetic resonance imaging in the detection of colorectal liver metastases. Ann R Coll Surg Engl 2008;90:25–28.

25. Sahani DV, Bajwa MA, Andrabi Y, Bajpai S, Cusack JC. Current status of imaging and emerging techniques to evaluate liver metastases from colorectal carcinoma. Ann Surg 2014;259:861–872.

26. O'Brien RT. Improved detection of metastatic hepatic hemangiosarcoma nodules with contrast ultrasound in three dogs. Vet Radiol and Ultrasound 2007;48:146–148.